Cell Reports

Report

Repurposing Pan-HDAC Inhibitors for *ARID1A*-Mutated Ovarian Cancer

Graphical Abstract

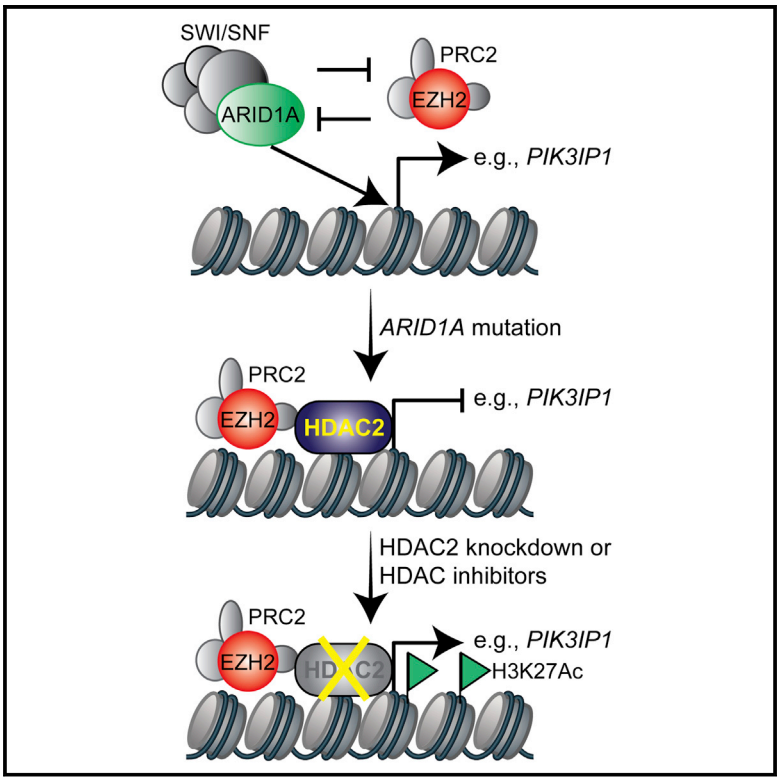

Highlights

- ARID1A inactivation enhanced growth suppression induced by HDAC2 inhibition
- HDAC2 interacts with EZH2 in an ARID1A status-dependent manner
- HDAC2 functions as a co-repressor of EZH2 to promote apoptosis
- SAHA improved the survival of mice bearing *ARID1A*-mutated cancer

Authors

Takeshi Fukumoto, Pyoung Hwa Park, Shuai Wu, ..., Jose R. Conejo-Garcia, Benjamin G. Bitler, Rugang Zhang

Correspondence

benjamin.bitler@ucdenver.edu (B.G.B.), rzhang@wistar.org (R.Z.)

In Brief

Fukumoto et al. show that *ARID1A* mutation confers sensitivity to pan-HDAC inhibitors such as SAHA in ovarian cancers. This correlated with enhanced growth suppression induced by the inhibition of HDAC2 activity in *ARID1A*-mutated cells. These findings provided preclinical rationales for repurposing FDA-approved pan-HDAC inhibitors for treating *ARID1A*-mutated cancers.

Data and Software Availability

GSE107201

Fukumoto et al., 2018, Cell Reports *22*, 3393–3400
March 27, 2018
https://doi.org/10.1016/j.celrep.2018.03.019

CellPress

Cell Reports
Report

Repurposing Pan-HDAC Inhibitors for *ARID1A*-Mutated Ovarian Cancer

Takeshi Fukumoto,[1] Pyoung Hwa Park,[1] Shuai Wu,[1] Nail Fatkhutdinov,[1,2] Sergey Karakashev,[1] Timothy Nacarelli,[1] Andrew V. Kossenkov,[3] David W. Speicher,[3,4] Stephanie Jean,[5] Lin Zhang,[6] Tian-Li Wang,[7] Ie-Ming Shih,[7] Jose R. Conejo-Garcia,[8] Benjamin G. Bitler,[1,9,*] and Rugang Zhang[1,10,*]

[1]Gene Expression and Regulation Program, The Wistar Institute, Philadelphia, PA 19104, USA
[2]Kazan Federal University, Kazan, Russia
[3]Center for Systems and Computational Biology, The Wistar Institute, Philadelphia, PA 19104, USA
[4]Molecular and Cellular Oncogenesis Program, The Wistar Institute, Philadelphia, PA 19104, USA
[5]Helen F. Graham Cancer Center & Research Institute, Newark, DE 19713, USA
[6]Department of Obstetrics and Gynecology, University of Pennsylvania Perelman School of Medicine, Philadelphia, PA 19104, USA
[7]Departments of Pathology and Gynecology and Obstetrics, Johns Hopkins Medical Institutions, Baltimore, MD 21231, USA
[8]Department of Immunology, Moffitt Cancer Center, Tampa, FL 33612, USA
[9]Present address: Department of Obstetrics and Gynecology, University of Colorado Anschutz Medical Campus, Research Complex-2, 3005, 12700 East 19th Avenue, Aurora, CO 80045, USA
[10]Lead Contact
*Correspondence: benjamin.bitler@ucdenver.edu (B.G.B.), rzhang@wistar.org (R.Z.)
https://doi.org/10.1016/j.celrep.2018.03.019

SUMMARY

***ARID1A*, a subunit of the SWI/SNF complex, is among the most frequently mutated genes across cancer types. *ARID1A* is mutated in more than 50% of ovarian clear cell carcinomas (OCCCs), diseases that have no effective therapy. Here, we show that *ARID1A* mutation confers sensitivity to pan-HDAC inhibitors such as SAHA in ovarian cancers. This correlated with enhanced growth suppression induced by the inhibition of HDAC2 activity in *ARID1A*-mutated cells. HDAC2 interacts with EZH2 in an ARID1A status-dependent manner. HDAC2 functions as a corepressor of EZH2 to suppress the expression of EZH2/ARID1A target tumor suppressor genes such as PIK3IP1 to inhibit proliferation and promote apoptosis. SAHA reduced the growth and ascites of the *ARID1A*-inactivated OCCCs in both orthotopic and genetic mouse models. This correlated with a significant improvement of survival of mice bearing *ARID1A*-mutated OCCCs. These findings provided preclinical rationales for repurposing FDA-approved pan-HDAC inhibitors for treating *ARID1A*-mutated cancers.**

INTRODUCTION

SWI/SNF chromatin remodeling complexes regulate gene transcription by changing chromatin accessibility through hydrolyzation of ATP (Wilson and Roberts, 2011). Cancer genome sequencing revealed that mutations in genes encoding for the subunits of the SWI/SNF complexes collectively occur in ~20% of all human cancers (Kadoch et al., 2013). For example, saturation analysis of The Cancer Genome Atlas (TCGA) cancer mutational profile finds that the *ARID1A* subunit of the SWI/SNF complex is among the genes that show the highest mutation rates across multiple cancer types (Lawrence et al., 2014). *ARID1A* is mutated in more than 50% of ovarian clear cell carcinomas (OCCCs) and 30% of ovarian endometrioid carcinomas (OECs) (Jones et al., 2010; Wiegand et al., 2010). *ARID1A* mutation is a known genetic driver of ovarian cancer. More than 90% of the *ARID1A* mutations observed in ovarian cancer are frameshift or nonsense mutations that result in the loss of ARID1A protein expression (Jones et al., 2010; Wiegand et al., 2010). Loss of ARID1A correlates with late-stage disease and predicts early recurrence of OCCC (Ye et al., 2016). OCCC ranks second as the cause of death from ovarian cancer and is associated with the worst prognosis among the major ovarian cancer subtypes when diagnosed at advanced stages (Chan et al., 2008; Mackay et al., 2010). For advanced-stage disease, there is no effective therapy. In Japan, its prevalence is higher than in western countries, with an estimated incidence of ~25% of ovarian cancers (Saito and Katabuchi, 2016). *ARID1A* is mutated in ~62% of Japanese OCCC patients (Murakami et al., 2017).

Histone deacetylases (HDACs) are established targets against cancers (West and Johnstone, 2014). Several HDAC inhibitors have been approved by the U.S. Food and Drug Administration (FDA) for treating hematopoietic malignancies. The most extensively studied and commonly used HDAC inhibitor is suberoylanilide hydroxamine (SAHA or vorinostat). SAHA is a nonselective pan-HDAC inhibitor and was the first FDA-approved HDAC inhibitor (Mann et al., 2007). HDAC2 belongs to class I HDACs that function to remove acetyl groups from histones to condense chromatin and repress transcription (West and Johnstone, 2014). High expression of HDAC2 is associated with poor outcomes in ovarian cancer (Weichert et al., 2008). However, whether HDAC2 can be explored as a therapeutic target for *ARID1A*-mutated cancers has never been investigated. Here we show that *ARID1A*-mutated ovarian cancers are selectively sensitive to HDAC2 inhibition. The HDAC inhibitor SAHA reduces the tumor burden of *ARID1A*-mutated ovarian cancer and improves the survival of mice bearing *ARID1A*-mutated ovarian cancers. Our findings provide scientific

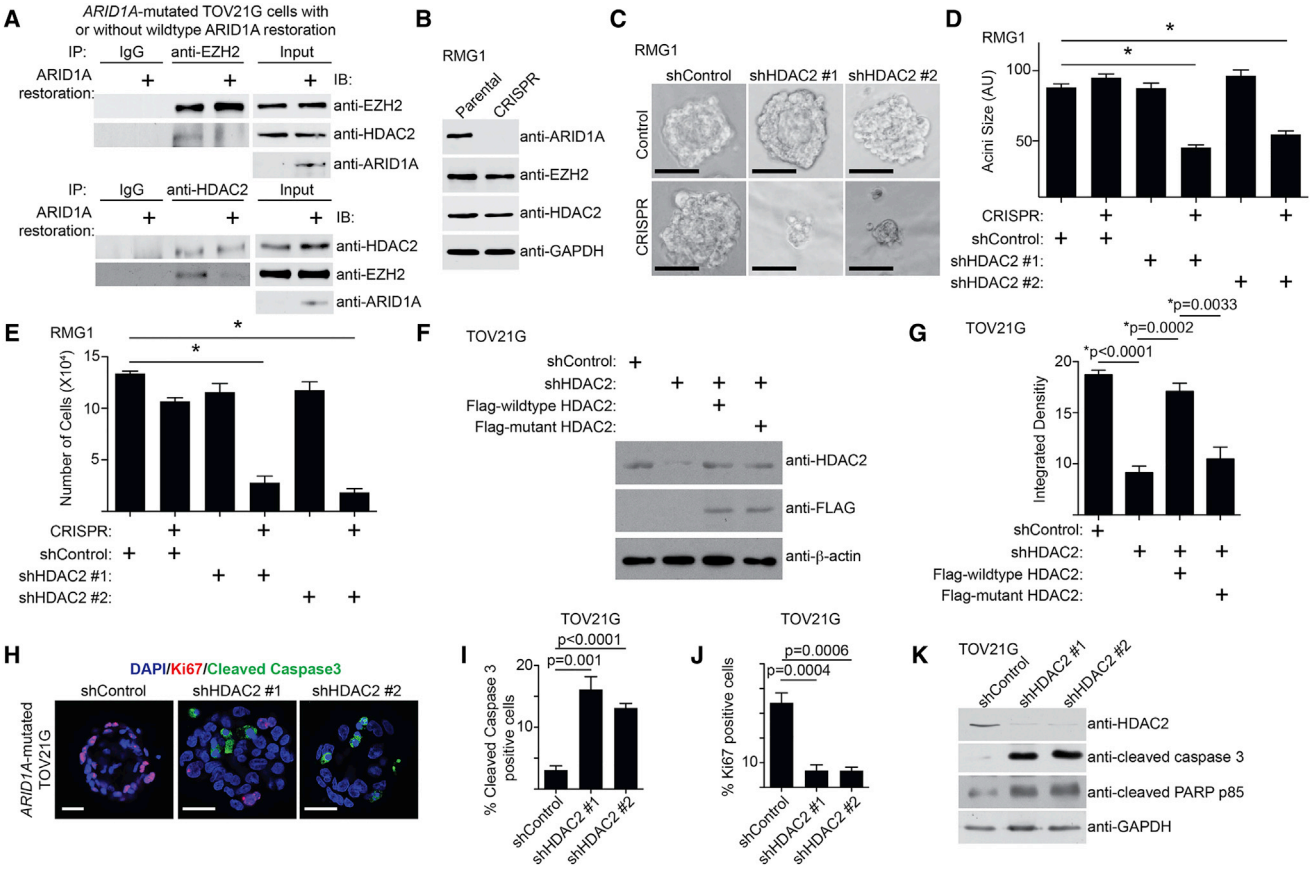

Figure 1. HDAC2 Inhibition Suppresses Cell Growth and Induces Apoptosis in ARID1A-Inactivated Cells

(A) *ARID1A*-mutated TOV21G cells with or without wild-type ARID1A restoration were subjected to co-immunoprecipitation (coIP) analysis using antibodies against EZH2 or HDAC2 or an immunoglobulin G (IgG) control. Immunoblots of the indicated proteins were performed.

(B) Immunoblot of the indicated proteins in parental and ARID1A CRISPR RMG1 cells.

(C) Indicated cells were grown in 3D using Matrigel. Scale bars, 75 measurable units (a.u.) using NIH ImageJ software.

(D) Quantification of the diameter of acini formed by the indicated cells in 3D culture. *$p < 0.05$. $n = 3$.

(E) Quantification of the number of cells recovered from 3D culture of the indicated cells. *$p < 0.05$. $n = 3$.

(F) *ARID1A*-mutated TOV21G cells with endogenous HDAC2 knockdown using a shRNA that targets the 3′ UTR region of the human *HDAC2* gene were concurrently expressing a FLAG-tagged, shRNA-resistant wild-type HDAC2 or a catalytically inactivated H142A HDAC2 mutant. Expression of HDAC2, FLAG, and β-actin was determined by immunoblot.

(G) Same as (F), but the indicated cells were subjected to growth analysis using the colony formation assay. Integrated density of colonies formed by the indicated cells was quantified. $n = 4$.

(H) Immunofluorescence staining of Ki67 (red), cleaved caspase-3 (green), and DAPI (blue) of the acini formed by *ARID1A*-mutated TOV21G cells with or without HDAC2 knockdown in 3D culture on day 12. Scale bars, 20 μm.

(I and J) Quantification of (H). 200 cells from each indicated group were examined for expression cleaved caspase-3 (I) or Ki67 (J). $n = 3$.

(K) *ARID1A*-mutated TOV21G cells with or without HDAC2 knockdown were examined for expression of markers of apoptosis cleaved caspase-3 and cleaved PARP p85, HDAC2, and GAPDH by immunoblot.

Error bars represent the SEM p value calculated with two-tailed t test. See also Figure S1.

rationale for repurposing FDA-approved HDAC inhibitors such as SAHA for *ARID1A*-mutated cancers.

RESULTS

HDAC2 Interacts with EZH2 in an ARID1A Status-Dependent Manner

Because EZH2 inhibition is synthetically lethal with *ARID1A* mutation (Bitler et al., 2015; Januario et al., 2017; Kim et al., 2015), and EZH2-containing PRC2 complex interacts with HDAC2 (van der Vlag and Otte, 1999), we sought to determine whether ARID1A regulates the interaction between EZH2 and HDAC2. Co-immunoprecipitation (coIP) analysis revealed that EZH2 and HDAC2 interact with each other in *ARID1A*-mutated TOV21G cells (Figure 1A). However, restoration of wild-type ARID1A impaired the interaction between EZH2 and HDAC2 (Figure 1A). EZH2 did not interact with HDAC2 in *ARID1A* wild-type RMG1 cells, whereas CRISPR-mediated knockout of ARID1A promoted their interaction (Figure S1A). As a control, there is no interaction based on coIP analysis between EZH2

and HDAC1 regardless of ARID1A status (Figure S1B). In addition, ARID1A does not interact with HDAC2 in *ARID1A* wild-type cells (Figure S1C). Consistent with previous reports (Helming et al., 2014), wild-type ARID1A restoration decreased the expression of ARID1B, the mutually exclusive subunit of ARID1A, in *ARID1A*-mutated cells (Figure S1D). However, HDAC2 did not interact with ARID1B in *ARID1A*-mutated cells (Figure S1E). Thus, we conclude that HDAC2 interacts with EZH2 in an ARID1A status-dependent manner.

HDAC2 Inhibition Suppresses Growth and Induces Apoptosis in ARID1A-Inactivated Cells

We next sought to determine whether ARID1A status affects response to HDAC2 inhibition. ARID1A knockout significantly enhanced the growth inhibition induced by HDAC2 knockdown in *ARID1A* wild-type RMG1 cells in both conventional two-dimensional (2D) cultures and three-dimensional (3D) cultures using Matrigel that more closely mimic the tumor environment (Figures 1B–1E, S1F, and S1G). Similar observations were made using additional *ARID1A* wild-type and mutated OCCC cell lines, as well as primary OCCC cultures from tumors with or without ARID1A expression (Figures S1H–S1R). Restoration of wild-type ARID1A in *ARID1A*-mutated cells de-sensitized these cells to HDAC2 knockdown (Figures S1S–S1V). We next sought to determine whether the observed sensitivity depends on the catalytic activity of HDAC2. The observed growth inhibition induced by HDAC2 knockdown can be rescued by a short hairpin RNA (shRNA)-resistant wild-type HDAC2, but not a mutant HDAC2 H142A that is deficient for its catalytic activity (Figures 1F, 1G, S1W, and S1X) (Kobayashi et al., 2017). Compared with ARID1A-proficient cells, ARID1A-deficient cells are more sensitive to CAY10683, a relatively selective tool HDAC2 inhibitor (Figure S1Y) (Pavlik et al., 2013). Altogether, we conclude that HDAC2 interacts with EZH2 in an ARID1A status-dependent manner, which correlates with the observed changes in sensitivity to inhibition of HDAC2 activity.

We next determined the expression of markers of apoptosis in *ARID1A* wild-type and mutated cells with or without HDAC2 knockdown by immunofluorescence staining of cleaved caspase-3, a marker of apoptosis, in acini formed in 3D culture (Figures 1H and S1Z). Cleaved caspase-3 was significantly induced by HDAC2 knockdown in *ARID1A*-mutated cells, but not wild-type cells (Figures 1I and S1AA). This was accompanied by a significant decrease in the cell proliferation marker Ki67 in *ARID1A*-mutated cells, but not wild-type cells (Figures 1J and S1AB). Immunoblot experiments revealed that markers of apoptosis such as cleaved caspase-3 and cleaved PARP p85 were significantly induced by HDAC2 knockdown in *ARID1A*-mutated cells, but not wild-type cells (Figures 1K and S1AC). Knockdown of EZH2- or HDAC2-induced growth inhibition and apoptosis were comparable, and there were no significant additive effects on growth inhibition or apoptosis induced by knockdown of EZH2 and HDAC2 (Figures S1AD–S1AE).

HDAC2 Regulates Expression of EZH2/ARID1A Target Gene *PIK3IP1*

To identify genes that are repressed by HDAC2, we performed RNA sequencing (RNA-seq) analysis in TOV21G cells with or without knockdown of HDAC2 expression by two independent short hairpin HDAC2s (shHDAC2s). RNA-seq analysis revealed that 1,111 genes were significantly upregulated by HDAC2 knockdown (GEO: GSE107201). Given that EZH2 and HDAC2 interaction is ARID1A status dependent and HDAC2 represses gene expression, we cross-referenced genes upregulated by HDAC2 knockdown with 45 EZH2/ARID1A target genes we have previously identified (Bitler et al., 2015). There is a significant enrichment of EZH2/ARID1A targets in genes upregulated by HDAC2 knockdown (Figure 2A). Among the identified genes, *PIK3IP1*, an inhibitor of phosphatidylinositol 3-kinase (PI3K)/AKT signaling (Zhu et al., 2007), plays a major role in apoptosis induced by EZH2 inhibition in *ARID1A*-mutated cells (Bitler et al., 2015). Thus, we explored whether HDAC2 regulates PIK3IP1 expression in an ARID1A status-dependent manner. HDAC2 knockdown induced PIK3IP1 expression in *ARID1A*-mutated cells, but not wild-type cells (Figures 2B and S2A). ARID1A knockout in *ARID1A* wild-type cells led to upregulation of PIK3IP1 by HDAC2 knockdown (Figure S2B), while wild-type ARID1A restoration in *ARID1A*-mutated cells suppressed HDAC2 knockdown-induced PIK3IP1 upregulation (Figure 2C). Consistent with previous reports (Weichert et al., 2008), compared with normal human ovarian surface epithelial cells, HDAC2 is expressed at higher levels in laser capture and micro-dissected OCCCs in a published dataset (Figure S2C) (Stany et al., 2011). Based on protein expression as determined by immunohistochemical (IHC) staining in 105 human OCCC and OEC specimens, HDAC2 negatively correlated with PIK3IP1 expression, while ARID1A positively correlated with PIK3IP1 expression (Figures 2D–2F). Altogether, these results support that HDAC2 and ARID1A antagonistically regulate PIK3IP1 expression.

We next determined the role of PIK3IP1 upregulation in mediating the observed sensitivity induced by HDAC2 inhibition. Toward this goal, we knocked down PIK3IP1 in HDAC2 knockdown, *ARID1A*-mutated TOV21G cells (Figure 2G). PIK3IP1 knockdown significantly impaired the growth inhibition induced by HDAC2 knockdown in both 2D and 3D cultures (Figures 2H–2J), which correlated with a suppression of apoptosis markers induced by HDAC2 knockdown (Figure 2G). Consistent with previous reports that PIK3IP1 suppresses PI3K/AKT signaling (Zhu et al., 2007), the observed changes correlated with the restoration of phosphor-AKT1 levels in PIK3IP1 knockdown cells (Figure 2G).

We next sought to determine whether HDAC2's association with the *PIK3IP1* gene promoter is regulated. Toward this goal, we performed chromatin immunoprecipitation (ChIP) analysis for HDAC2 in *ARID1A* wild-type RMG1 cells with or without ARID1A knockout. There is no significant association of HDAC2 with the PIK3IP1 gene promoter in *ARID1A* wild-type cells (Figure 3A). In contrast, ARID1A knockout led to a significant increase in the association of HDAC2 with the *PIK3IP1* gene promoter (Figure 3B). HDAC2 knockdown significantly increased H3K27ac on the *PIK3IP1* gene promoter in ARID1A knockout cells, but not *ARID1A* wild-type cells (Figures 3A and 3B). This correlates with a significant increase in the association of RNA polymerase II (Pol II) with the *PIK3IP1* gene promoter in ARID1A knockout cells, but not *ARID1A* wild-type cells (Figures 3A and

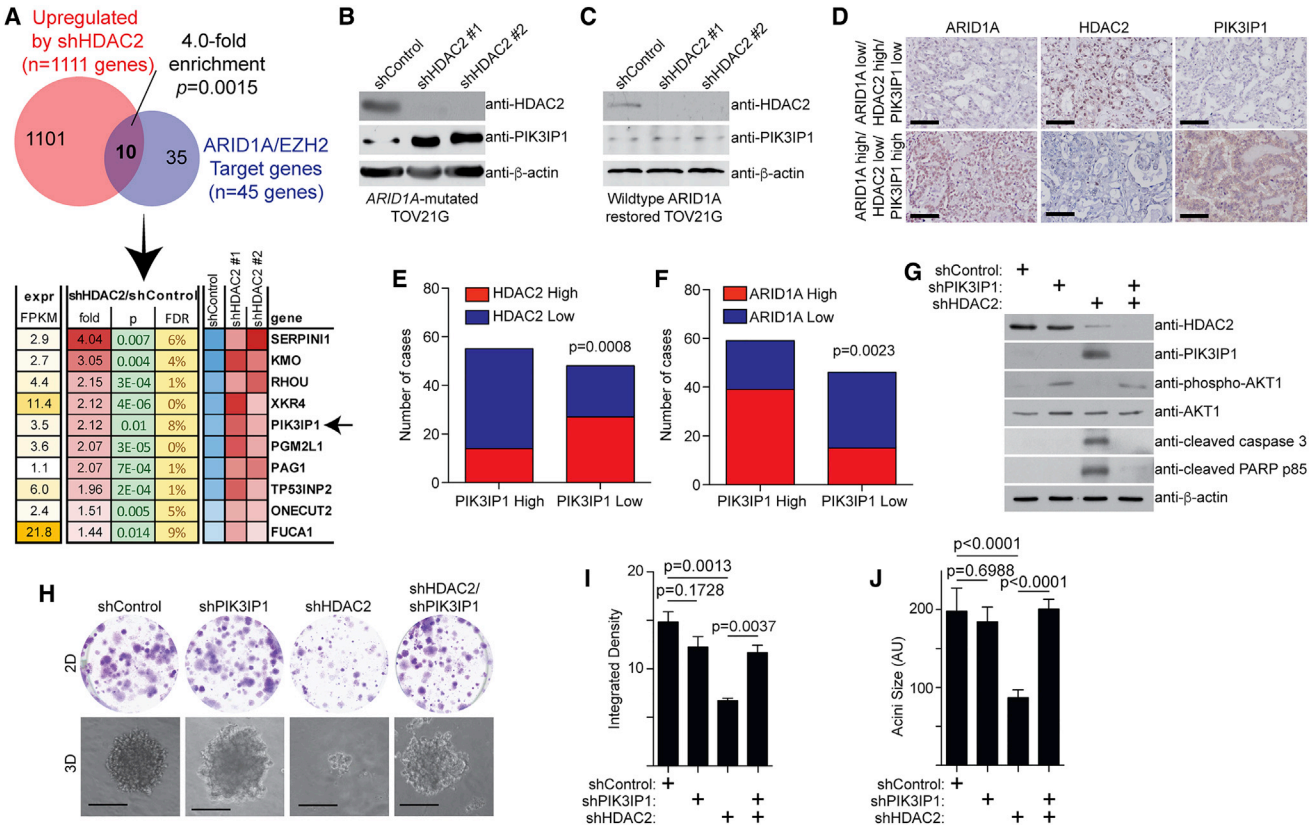

Figure 2. HDAC2 and ARID1A Antagonistically Regulate PIK3IP1 Expression

(A) *ARID1A*-mutated TOV21G cells expressing two independent shHDAC2s or control were subjected to RNA-seq analysis. The genes upregulated by both shHDAC2s were cross-referenced with ARID1A/EZH2 target genes (Bitler et al., 2015).

(B and C) Immunoblot of the indicated proteins in *ARID1A*-mutated TOV21G without (B) or with (C) wild-type ARID1A restoration with or without HDAC2 knockdown by two independent shHDAC2s.

(D) Representative images of immunohistochemical staining using the indicated antibodies in 105 human ovarian clear cell carcinoma (OCCC) and ovarian endometrioid carcinoma (OEC) specimens. Scale bar, 100 μm.

(E and F) Quantification of (D). Expression of PIK3IP1, ARID1A, and HDAC2 was scored as high or low based on histological scores (H-scores). An H-score higher than the median of H-scores was considered high, and one lower than the median of H-scores was considered low. Correlation between HDAC2 and PIK3IP1 expression (E) and between ARID1A and PIK3IP1 (F) was examined. The p value was calculated by two-tailed Fisher's exact test.

(G–J) Immunoblot of the indicated proteins in *ARID1A*-mutated TOV21G cells expressing shHDAC2, shPIK3IP1, or a combination (G). The indicated cells were subjected to 2D colony formation assay and 3D growth using Matrigel (H). Scale bar, 75 measurable units (a.u.) using NIH ImageJ software. n = 3. Integrated density of colonies formed in 2D was quantified (I). n = 4. The diameter of acini formed by the indicated cells in 3D was quantified (J). n = 3. Error bars represent the SEM p value calculated with two-tailed t test.

See also Figure S2.

3B). Consistent with previous reports (Bitler et al., 2015), EZH2's association with the *PIK3IP1* gene promoter was not affected by ARID1A status (Figures S3A and S3B). Similar to what we observed in ARID1A knockout cells, HDAC2's association with the *PIK3IP1* gene promoter was reduced by HDAC2 knockdown in *ARID1A*-mutated cells (Figure 3C). This correlated with an increase in H3K27ac and RNA Pol II's association with the *PIK3IP1* gene promoter in *ARID1A*-mutated TOV21G cells (Figure 3C). In contrast, there were no changes in EZH2's association with the *PIK3IP1* gene promoter in *ARID1A*-mutated TOV21G cells (Figure S3C). HDAC2's association with the *PIK3IP1* promoter was not affected by knockdown of EZH2 (Figure S3D) or ARID1B in *ARID1A*-mutated TOV21G cells (Figures S3E and S3F). Altogether, these data support a model whereby ARID1A prevents the binding of HDAC2 to the *PIK3IP1* gene promoter (Figure S3G). This model is consistent with the findings that HDAC2 and EZH2 interact with each other in *ARID1A*-mutated cells, but not wild-type cells.

SAHA Reduced Tumor Burden and Improved Survival of Mice Bearing *ARID1A*-Inactivated Ovarian Cancers

There is no selective HDAC2 inhibitor available for *in vivo* animal studies. Thus, we explored the therapeutic potential for SAHA, an FDA-approved pan-HDAC inhibitor that is suitable for *in vivo* animal studies (Mann et al., 2007), in *ARID1A*-mutated ovarian cancers of preclinical models. Compared with *ARID1A* wild-type cells, the half maximal inhibitory concentration (IC_{50}) of SAHA is significantly lower in *ARID1A*-mutated cells (Figure 4A; Table S1).

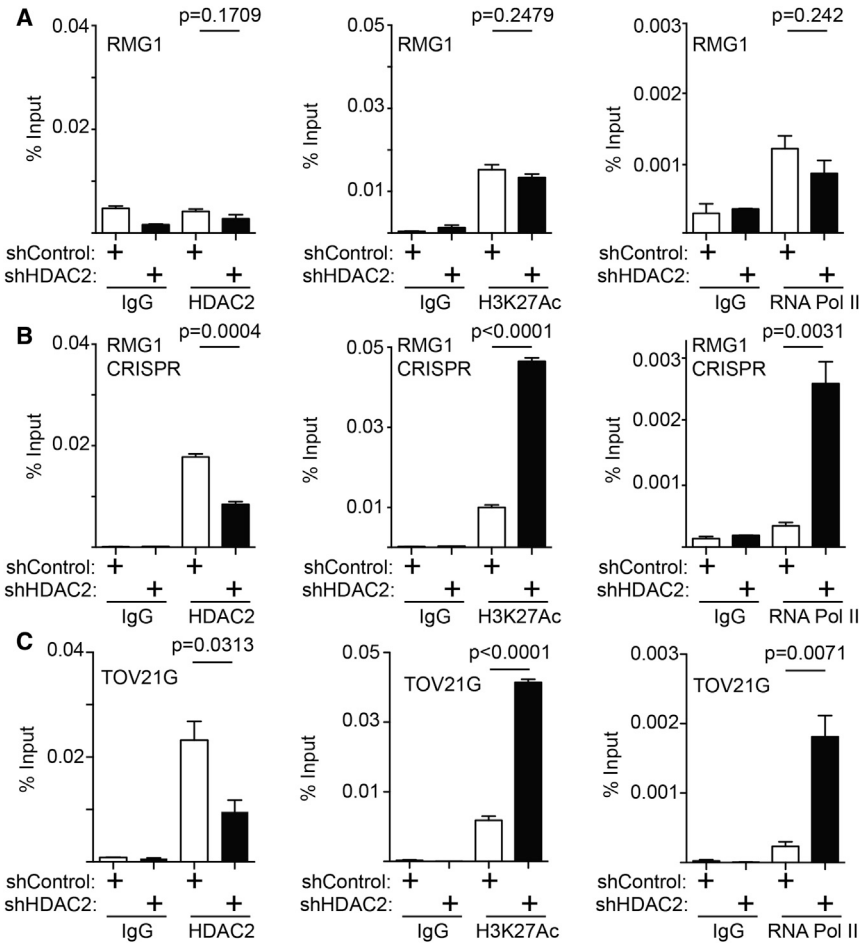

Figure 3. HDAC2 Directly Regulates *PIK3IP1* Gene in an ARID1A Status-Dependent Manner

(A–C) *ARID1A* wild-type RMG1 cells (A), ARID1A CRISPR RMG1 cells (B), and *ARID1A*-mutated TOV21G cells (C) with or without HDAC2 knockdown were subjected to ChIP analysis for the *PIK3IP1* gene promoter using the indicated antibodies. An isotype-matched IgG was used as a control. n = 4. Error bars represent the SEM p value calculated with two-tailed t test. See also Figure S3.

To determine the effects of HDAC2 inhibition *in vivo* on the growth of *ARID1A*-mutated tumors, we orthotopically transplanted luciferase-expressing *ARID1A*-mutated TOV21G cells into the bursa sac covering the ovary of immunocompromised nude mice to mimic the tumor microenvironment. The injected *ARID1A* wild-type or mutant cells were allowed to grow for 1 week to establish the orthotopic tumors. Mice were then randomized and treated daily for 3 weeks with vehicle control or SAHA (50 mg/kg) by intraperitoneal (i.p.) injection at the same dose as previously reported (Butler et al., 2000). SAHA treatment significantly inhibited the growth of xenografted *ARID1A*-mutated tumors (Figures S4A and S4B). We next examined the effects of SAHA treatment on the tumor burden of the transplanted *ARID1A*-mutated cells. Using tumor weight as a surrogate, we found that SAHA treatment significantly reduced the burden of orthotopically xenografted *ARID1A*-mutated tumors (Figures 4B and 4C). Malignant ascites presents a considerable clinical challenge to the management of ovarian cancer (Kipps et al., 2013). Thus, we examined the effects of SAHA treatment on ascites production. SAHA significantly reduced the amount of ascites formed in mice bearing *ARID1A*-mutated tumors (Figures 4D and 4E). We next followed the survival of the treated mice after discontinuing the treatment regimens. Compared with vehicle controls, SAHA significantly improved the survival of mice bearing the orthotopically transplanted *ARID1A*-mutated tumors (Figure 4F). Likewise, SAHA significantly suppressed tumor growth, reduced the amount of ascites, and improved the survival in the pre-established, conditional *Arid1a*$^{-/-}$/*Pik3ca*^{H1047R}-immunocompetent genetic OCCC mouse model (Figures 4G–4L). As a control, SAHA did not significantly affect the growth of orthotopically transplanted *ARID1A* wild-type RMG1 tumors (Figures S4C and S4D). Thus, we conclude that SAHA significantly improved the survival of mice bearing *ARID1A*-mutated ovarian tumors.

Finally, we sought to correlate the observed improvement of survival, suppression of tumor growth, and reduction in tumor burden *in vivo* with the molecular pathways we have revealed *in vitro*. To do so, we performed IHC analysis for markers of cell proliferation (Ki67), apoptosis (cleaved caspase-3), and PIK3IP1 in the dissected *ARID1A*-mutated tumors treated with SAHA or controls. SAHA significantly decreased the cell proliferation marker Ki67 and increased the apoptotic marker cleaved caspase-3 (Figures 4M and 4N). Furthermore, PIK3IP1 staining was significantly increased by SAHA treatment (Figures 4M and 4N). *ARID1A*-mutated tumors also depend on HDAC6 activity, which is due to the deacetylation of pro-apoptotic lysine 120 residue of p53 (p53K120ac) by HDAC6 (Bitler et al., 2017). However, the dose of SAHA used in the present study did not significantly affect p53K120ac levels, suggesting that the observed anti-tumor effects are independent of HDAC6 (Figures S4E and S4F). Altogether, we conclude that SAHA suppresses the growth of *ARID1A*-mutated ovarian tumors, which correlates with a decrease in cell proliferation, an increase in apoptosis, and an upregulation of HDAC2/ARID1A target gene PIK3IP1 in the treated *ARID1A*-mutated tumors.

DISCUSSION

Here, we show that *ARID1A*-mutated ovarian cancer cells are sensitive to HDAC2 inhibition. This correlates with the recruitment of HDAC2 to the ARID1A/EZH2 target genes such as

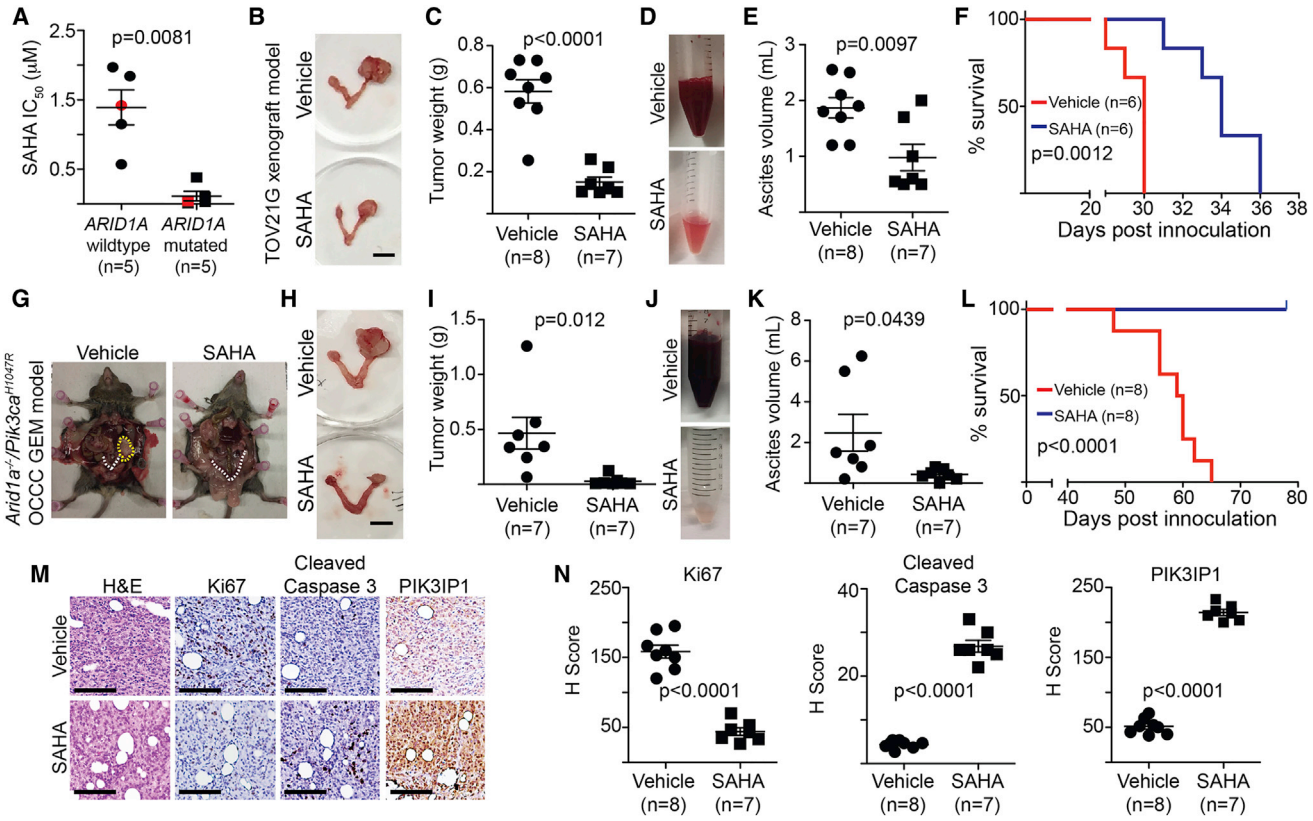

Figure 4. SAHA Reduced Tumor Burden and Improved Survival of Mice Bearing *ARID1A*-Inactivated Ovarian Cancers

(A) The IC_{50} of SAHA is significantly higher in *ARID1A* wild-type cells than in mutated cells. Red labels indicate primary OCCC cultures.

(B–F) Mice with established TOV21G tumors were randomized and treated with vehicle control or SAHA (50 mg/kg) daily by i.p. injection for 3 weeks. Representative images of reproductive tracks with tumors treated with vehicle control or SAHA (B). Scale bar, 10 mm. Tumor weigh was quantified and used as a surrogate for tumor burden (C). Representative images of ascites collected from the mice treated with vehicle control or SAHA (D). The volume of ascites produced was quantified (E). After stopping the treatment, the mice from the indicated groups were followed for survival (F).

(G–L) *Pik3ca*^{H1047R}/*Arid1a*$^{flox/flox}$-driven OCCCs were allowed to establish for 5 weeks and then were randomized and treated daily with 50 mg/kg of i.p. SAHA or vehicle control for 3 weeks. Representative images of mice treated with vehicle control or SAHA (G). White dashed lines indicate reproduction tracks, and the yellow dashed circle indicates the tumor formed. Images of dissected reproductive tracks with tumors from mice treated with vehicle control or SAHA (H). Scale bar, 10 mm. Tumor weigh was quantified and used as a surrogate for tumor burden (I). Representative images of ascites collected from the mice treated with vehicle control or SAHA (J). The volume of ascites produced was quantified (K). After stopping the treatment, the mice from the indicated groups were followed for survival (L).

(M and N) Same as (B). The consecutive sections of the xenograft tumors dissected from the indicated treatment groups were subjected to immunohistochemical staining using the indicated antibodies (M). Scale bar, 50 μm. H-score was quantified (N).

Error bars represent the SEM p value calculated with two-tailed t test. See also Figure S4 and Table S1.

PIK3IP1 in an ARID1A status-dependent manner. HDAC2 and EZH2 interact with each other in ARID1A-deficient cells, but not in ARID1A-proficient cells. This supports the notion that the presence of ARID1A in the ARID1A/EZH2 target gene promoters prevented the recruitment of HDAC2 to these loci (Figure S3G). Growth inhibition and apoptosis induced by HDAC2 and EZH2 inhibition are comparable in *ARID1A*-mutated cells. However, it might be advantageous to inhibit HDAC2 and EZH2 activity simultaneously to prevent the development of resistance to inhibition of either HDAC2 or EZH2 alone. HDAC2 does not interact with either ARID1A or ARID1B. However, it is possible that ARID1A is mutually exclusive to an HDAC2-containing complex other than HDAC2-EZH2. We previously showed that *ARID1A*-mutated ovarian cancers depend on HDAC6 activity due to direct suppression of *HDAC6* gene by ARID1A (Bitler et al., 2017). In *ARID1A* wild-type cells, HDAC2 knockdown did not show selectivity against shRNA-mediated ARID1A knockdown (Bitler et al., 2017). In contrast, here we showed that compared with *ARID1A* wild-type cells, CRISPR-mediated ARID1A knockout cells are more sensitive to HDAC2 knockdown (Figures 2B–2E). This highlighted the advantage of performing analysis in complete-knockout cells compared to partial-knockdown cells. In addition to HDAC2, pan-HDAC inhibitors inhibit the activities of other HDACs that are equally effective in suppressing both ARID1A-deficient and ARID1A-proficient cells (Bitler et al., 2017). However, the IC_{50} of SAHA is significantly lower in *ARID1A*-mutated cells compared with *ARID1A* wild-type cells (Figure 4A). This

suggests selectivity can be achieved with pan-HDAC inhibitors in ARID1A-inactivated cells.

In summary, our studies demonstrate that targeting HDAC2 activity using pan-HDAC inhibitors such as SAHA in *ARID1A*-mutated cells represents an urgently needed therapeutic strategy. SAHA is FDA approved. Thus, our studies provide a scientific rationale for a potential translation of these findings by repurposing the FDA-approved pan-HDAC inhibitors such as SAHA for *ARID1A*-mutated ovarian cancers, for which no effective therapies exist. Given that mutation and loss of expression of ARID1A and genetic alterations in other subunits of ATP-dependent chromatin remodeling complexes are observed in ~20% of all human cancers (Kadoch et al., 2013), our findings may have far-reaching implications for improving therapy for an array of cancer types.

EXPERIMENTAL PROCEDURES

ChIP

ChIP was performed as previously described (Bitler et al., 2015). The following antibodies were used to perform ChIP: anti-HDAC2 (Abcam), anti-H3K27ac (Millipore), anti-Pol II (Santa Cruz), and anti-EZH2 (Cell Signaling). Isotype-matched immunoglobulin G was used as a negative control. ChIP DNA was analyzed by qPCR against the promoter of the human *PIK3IP1* gene using the following primers: forward, 5′-AGGTGATTGAACGACCAGTG-3′, and reverse, 5′-GGGAAGCTCCCAGTTCTAAAG-3′.

Orthotopic Xenograft Ovarian Cancer Mouse Models *In Vivo*

The protocols were approved by the Institutional Animal Care and Use Committee (IACUC). For *in vivo* experiments, the sample size of mice per group was determined based on the data shown from *in vitro* experiments. Intrabursal orthotopic xenograft was performed as described previously (Bitler et al., 2015). Briefly, 1 × 10^6 luciferase-expressing, *ARID1A*-mutated TOV21G or *ARID1A* wild-type RMG1 cells were unilaterally injected into the ovarian bursa sac of 6- to 8-week-old female immunocompromised NOD scid gamma mice (NSG) mice. One week after injection of TOV21G cells, we visualized tumors by injecting luciferin (i.p.; 4 mg per mouse) resuspended in PBS and imaged with an In Vivo Imaging System (IVIS) Spectrum imaging system. The mice were then randomized into two groups based on luciferase activity and treated with vehicle control (2% DMSO/30% polyethylene glycol [PEG] 300/double distilled water [ddH_2O]) or SAHA (50 mg/kg) daily by i.p. injection for an additional 3 weeks. Images were analyzed using Live Imaging 4.0 software. Imaging analysis was performed blindly, but not randomly. Animal experiments were randomized. There was no exclusion from the experiments.

Arid1a$^{-/-}$/*Pik3ca*^{H1047R} Genetic Clear Cell Ovarian Tumor Mouse Model

All experiments were approved by the IACUC. Transgenic mice with latent mutations in *Arid1a* and *Pik3ca* were generated by crossing *Arid1a*$^{flox/flox}$ mice (provided by Dr. Wang, University of Michigan, and crossed onto a C57BL/6J background for 9 generations) with R26-*Pik3ca*^{H1047R} mice carrying inducible *Pik3ca* mutations (Jackson Laboratory, Jax 016977) as previously described (Bitler et al., 2017). All mice were maintained in specific pathogen-free barrier facilities. To induce tumorigenesis, 6- to 10-week-old *Pik3ca*^{H1047R}/*Arid1a*$^{-/-}$ female mice were intrabursally injected with adenovirus-Cre as previously described (Bitler et al., 2017). 5 weeks after adenovirus-Cre injection, mice with palpable tumors were randomized and treated with SAHA (50 mg/kg) or vehicle control for 21 days. Following treatment, mice were sacrificed and the tumors were surgically dissected or followed for survival.

Statistical Analysis

Statistical analyses were performed using GraphPad Prism 6 (GraphPad) for Mac OS. Quantitative data are expressed as mean ± SEM unless otherwise stated. ANOVA with Fisher's least significant difference was used to identify significant differences among multiple groups. For all statistical analyses, the level of significance was set at 0.05.

DATA AND SOFTWARE AVAILABILITY

The accession number for the RNA-sequence data reported in this paper is GEO: GSE107201.

SUPPLEMENTAL INFORMATION

Supplemental Information includes Supplemental Experimental Procedures, four figures, and one table and can be found with this article online at https://doi.org/10.1016/j.celrep.2018.03.019.

ACKNOWLEDGMENTS

We thank Dr. Cigall Kadoch for the ARID1A CRISPR plasmid and Drs. David Hunstman and Yemin Wang for primary ovarian clear cell carcinoma cultures. This work was supported by the NIH (R01CA160331, R01CA163377, and R01CA202919 to R.Z. and R00CA194318 to B.G.B.), the U.S. Department of Defense (OC140632P1 and OC150446 to R.Z.), and an Ovarian Cancer Research Fund Alliance (OCRFA) program project (#291009 to R.Z.). Support of core facilities was provided by a Cancer Centre Support Grant (CCSG) (CA010815) to The Wistar Institute.

AUTHOR CONTRIBUTIONS

T.F., P.H.P., S.W., N.F., S.K., and T.N. performed the experiments and analyzed data. B.G.B. and R.Z. designed the experiments. A.V.K. performed the bioinformatics analysis. D.W.S., S.J., L.Z., and J.R.C.-G. participated in the experimental design. T.-L.W. and I.-M.S. contributed key reagents. T.F., B.G.B., J.R.C.-G., and R.Z. wrote the manuscript. R.Z. conceived the study.

DECLARATION OF INTERESTS

The authors declare no competing interests.

Received: December 12, 2017
Revised: February 13, 2018
Accepted: March 1, 2018
Published: March 27, 2018

REFERENCES

Bitler, B.G., Aird, K.M., Garipov, A., Li, H., Amatangelo, M., Kossenkov, A.V., Schultz, D.C., Liu, Q., Shih, IeM., Conejo-Garcia, J.R., et al. (2015). Synthetic lethality by targeting EZH2 methyltransferase activity in ARID1A-mutated cancers. Nat. Med. *21*, 231–238.

Bitler, B.G., Wu, S., Park, P.H., Hai, Y., Aird, K.M., Wang, Y., Zhai, Y., Kossenkov, A.V., Vara-Ailor, A., Rauscher, F.J., III., et al. (2017). ARID1A-mutated ovarian cancers depend on HDAC6 activity. Nat. Cell Biol. *19*, 962–973.

Butler, L.M., Agus, D.B., Scher, H.I., Higgins, B., Rose, A., Cordon-Cardo, C., Thaler, H.T., Rifkind, R.A., Marks, P.A., and Richon, V.M. (2000). Suberoylanilide hydroxamic acid, an inhibitor of histone deacetylase, suppresses the growth of prostate cancer cells *in vitro* and *in vivo*. Cancer Res. *60*, 5165–5170.

Chan, J.K., Teoh, D., Hu, J.M., Shin, J.Y., Osann, K., and Kapp, D.S. (2008). Do clear cell ovarian carcinomas have poorer prognosis compared to other epithelial cell types? A study of 1411 clear cell ovarian cancers. Gynecol. Oncol. *109*, 370–376.

Helming, K.C., Wang, X., Wilson, B.G., Vazquez, F., Haswell, J.R., Manchester, H.E., Kim, Y., Kryukov, G.V., Ghandi, M., Aguirre, A.J., et al. (2014). ARID1B is a specific vulnerability in ARID1A-mutant cancers. Nat. Med. *20*, 251–254.

Januario, T., Ye, X., Bainer, R., Alicke, B., Smith, T., Haley, B., Modrusan, Z., Gould, S., and Yauch, R.L. (2017). PRC2-mediated repression of SMARCA2

predicts EZH2 inhibitor activity in SWI/SNF mutant tumors. Proc. Natl. Acad. Sci. USA *114*, 12249–12254.

Jones, S., Wang, T.L., Shih, IeM., Mao, T.L., Nakayama, K., Roden, R., Glas, R., Slamon, D., Diaz, L.A., Jr., Vogelstein, B., et al. (2010). Frequent mutations of chromatin remodeling gene ARID1A in ovarian clear cell carcinoma. Science *330*, 228–231.

Kadoch, C., Hargreaves, D.C., Hodges, C., Elias, L., Ho, L., Ranish, J., and Crabtree, G.R. (2013). Proteomic and bioinformatic analysis of mammalian SWI/SNF complexes identifies extensive roles in human malignancy. Nat. Genet. *45*, 592–601.

Kim, K.H., Kim, W., Howard, T.P., Vazquez, F., Tsherniak, A., Wu, J.N., Wang, W., Haswell, J.R., Walensky, L.D., Hahn, W.C., et al. (2015). SWI/SNF-mutant cancers depend on catalytic and non-catalytic activity of EZH2. Nat. Med. *21*, 1491–1496.

Kipps, E., Tan, D.S., and Kaye, S.B. (2013). Meeting the challenge of ascites in ovarian cancer: new avenues for therapy and research. Nat. Rev. Cancer *13*, 273–282.

Kobayashi, T., Nakazono, K., Tokuda, M., Mashima, Y., Dynlacht, B.D., and Itoh, H. (2017). HDAC2 promotes loss of primary cilia in pancreatic ductal adenocarcinoma. EMBO Rep. *18*, 334–343.

Lawrence, M.S., Stojanov, P., Mermel, C.H., Robinson, J.T., Garraway, L.A., Golub, T.R., Meyerson, M., Gabriel, S.B., Lander, E.S., and Getz, G. (2014). Discovery and saturation analysis of cancer genes across 21 tumour types. Nature *505*, 495–501.

Mackay, H.J., Brady, M.F., Oza, A.M., Reuss, A., Pujade-Lauraine, E., Swart, A.M., Siddiqui, N., Colombo, N., Bookman, M.A., Pfisterer, J., et al. (2010). Prognostic relevance of uncommon ovarian histology in women with stage III/IV epithelial ovarian cancer. Int. J. Gynecol. Cancer *20*, 945–952.

Mann, B.S., Johnson, J.R., Cohen, M.H., Justice, R., and Pazdur, R. (2007). FDA approval summary: vorinostat for treatment of advanced primary cutaneous T-cell lymphoma. Oncologist *12*, 1247–1252.

Murakami, R., Matsumura, N., Brown, J.B., Higasa, K., Tsutsumi, T., Kamada, M., Abou-Taleb, H., Hosoe, Y., Kitamura, S., Yamaguchi, K., et al. (2017). Exome sequencing landscape analysis in ovarian clear cell carcinoma shed light on key chromosomal regions and mutation gene networks. Am. J. Pathol. *187*, 2246–2258.

Pavlik, C.M., Wong, C.Y., Ononye, S., Lopez, D.D., Engene, N., McPhail, K.L., Gerwick, W.H., and Balunas, M.J. (2013). Santacruzamate A, a potent and selective histone deacetylase inhibitor from the Panamanian marine cyanobacterium cf. *Symploca* sp. J. Nat. Prod. *76*, 2026–2033.

Saito, T., and Katabuchi, H. (2016). Annual report of the Committee on Gynecologic Oncology, Japan Society of Obstetrics and Gynecology: patient annual report for 2013 and treatment annual report for 2008. J. Obstet. Gynaecol. Res. *42*, 1069–1079.

Stany, M.P., Vathipadiekal, V., Ozbun, L., Stone, R.L., Mok, S.C., Xue, H., Kagami, T., Wang, Y., McAlpine, J.N., Bowtell, D., et al. (2011). Identification of novel therapeutic targets in microdissected clear cell ovarian cancers. PLoS ONE *6*, e21121.

van der Vlag, J., and Otte, A.P. (1999). Transcriptional repression mediated by the human polycomb-group protein EED involves histone deacetylation. Nat. Genet. *23*, 474–478.

Weichert, W., Denkert, C., Noske, A., Darb-Esfahani, S., Dietel, M., Kalloger, S.E., Huntsman, D.G., and Köbel, M. (2008). Expression of class I histone deacetylases indicates poor prognosis in endometrioid subtypes of ovarian and endometrial carcinomas. Neoplasia *10*, 1021–1027.

West, A.C., and Johnstone, R.W. (2014). New and emerging HDAC inhibitors for cancer treatment. J. Clin. Invest. *124*, 30–39.

Wiegand, K.C., Shah, S.P., Al-Agha, O.M., Zhao, Y., Tse, K., Zeng, T., Senz, J., McConechy, M.K., Anglesio, M.S., Kalloger, S.E., et al. (2010). ARID1A mutations in endometriosis-associated ovarian carcinomas. N. Engl. J. Med. *363*, 1532–1543.

Wilson, B.G., and Roberts, C.W. (2011). SWI/SNF nucleosome remodellers and cancer. Nat. Rev. Cancer *11*, 481–492.

Ye, S., Yang, J., You, Y., Cao, D., Huang, H., Wu, M., Chen, J., Lang, J., and Shen, K. (2016). Clinicopathologic significance of HNF-1β, AIRD1A, and PIK3CA expression in ovarian clear cell carcinoma: a tissue microarray study of 130 cases. Medicine (Baltimore) *95*, e3003.

Zhu, Z., He, X., Johnson, C., Stoops, J., Eaker, A.E., Stoffer, D.S., Bell, A., Zarnegar, R., and DeFrances, M.C. (2007). PI3K is negatively regulated by PIK3IP1, a novel p110 interacting protein. Biochem. Biophys. Res. Commun. *358*, 66–72.

Cell Reports, Volume *22*

Supplemental Information

Repurposing Pan-HDAC Inhibitors for *ARID1A*-Mutated Ovarian Cancer

Takeshi Fukumoto, Pyoung Hwa Park, Shuai Wu, Nail Fatkhutdinov, Sergey Karakashev, Timothy Nacarelli, Andrew V. Kossenkov, David W. Speicher, Stephanie Jean, Lin Zhang, Tian-Li Wang, Ie-Ming Shih, Jose R. Conejo-Garcia, Benjamin G. Bitler, and Rugang Zhang

Supplemental Figures and Figure Legends

Supplemental Figure 1

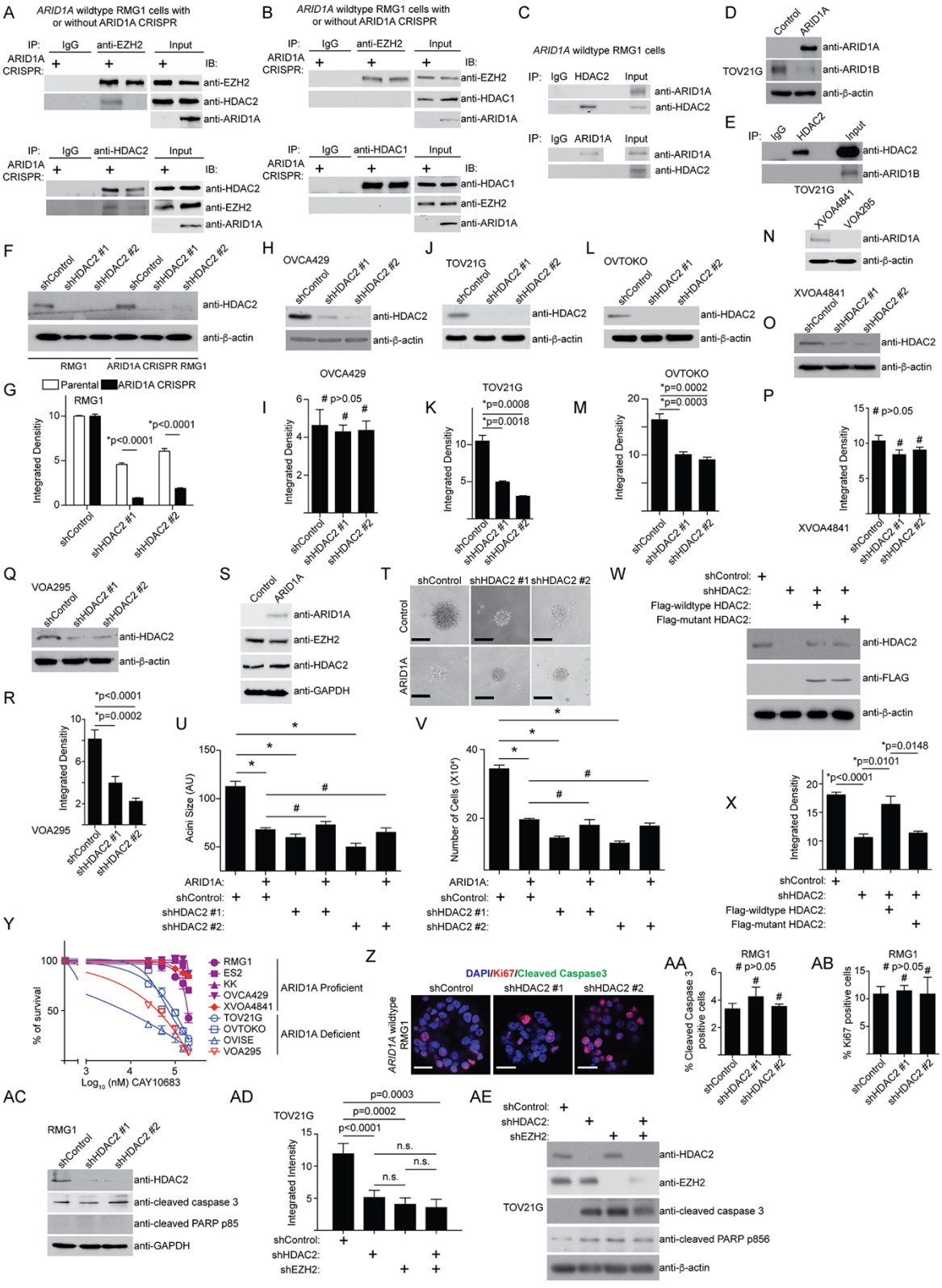

Supplemental Figure 1. HDAC2 inhibition is selective against ARID1A inactivation. Related to Figure 1.

(**A**) Parental *ARID1A* wildtype RMG1 or ARID1A CRISPR knockout RMG1 cells were subjected to co-IP analysis using antibodies against EZH2 or HDAC2. An isotype matched IgG was used as a negative control. Immunoblots of the indicated proteins were performed. (**B-C**) Same as (A), but the cells were subjected to co-IP analysis using antibodies against EZH2 or HDAC1 (B), or using antibodies against ARID1A or HDAC2. An isotype matched IgG was used as a negative control. (**D**) Expression of ARID1A, ARID1B and a loading control β-actin was determined by immunoblot in *ARID1A*-mutated TOV21G cells with or without wildtype ARID1A restoration. (**E**) *ARID1A*-mutated TOV21G cells were subjected to co-IP analysis using antibodies against HDAC2. An isotype matched IgG was used as a negative control. Immunolots of the indicated proteins were performed. (**F-G**) *ARID1A* wildtype RMG1 cells were transduced with lentivirus encoding the indicated shHDAC2s or control. Expression of HDAC2 and a loading control β-actin was determined by immunoblot (F). The indicated cells were subjected to colony formation assay. Integrated density of colonies formed by the indicated cells were quantified using the NIH Image J software (G). n=4 independent experiments. (**H-M**) Same as (F-G), but for *ARID1A* wildtype OVCA429 cells (H-I), *ARID1A*-mutated TOV21G (J-K) or OVTOKO (L-M) cells. n=4 independent experiments. (**N**) Expression of ARID1A and a loading control β-actin was determined by immunoblot in the indicated primary cultures of human ovarian clear cell carcinoma (OCCC) cells. (**O-R**) Same as (F-G), but for the indicated primary cultures of human OCCC cells. (**S-V**) Immunoblot of the indicated proteins in *ARID1A*-mutated TOV21G cells with or without wildtype ARID1A restoration (S). The indicated cells were grown in 3D Matrigel. Shown are representative images of acini formed by the indicated cells (T). Scale Bars = 75 measurable units (a.u.) using the NIH Image J software. The diameter of acini formed by the indicated cells in 3D culture was quantified using NIH Image J software (U). $^{\#}P > 0.05$, $*P < 0.05$. n=3 independent experiments. Numbers of cells recovered from 3D cultures of the indicated cells were quantified (V). $^{\#}P > 0.05$, $*P < 0.05$. n=4 independent experiments. (**W-X**) *ARID1A*-mutated OVISE cells with endogenous HDAC2 knockdown using a shRNA that targets the 3' UTR region of the human *HDAC2* gene were concurrently expressing a FLAG-tagged shRNA resistant wildtype HDAC2 or a catalytically inactivated H142A HDAC2 mutant. Expression of HDAC2, FLAG, and a loading control β-actin was determined by immunoblot (W). The indicated cells were subjected to growth analysis using the colony formation assay. Quantification of integrated density of colonies formed by the indicated cells using the NIH Image J software (X). n=4 independent experiments. Error bars represent SEM. *P*-value calculated with two-tailed *t*-test. (**Y**) Dose-responsive curves of CAY10683, a relative selective tool HDAC2 inhibitor (Pavlik et al., 2013), in the indicated *ARID1A* proficient cells and deficient cells. Error bars represent SEM. (**Z**) Immunofluorescence staining of Ki67 (red), cleaved caspase 3 (green), and DAPI (blue) for the acini formed by *ARID1A* wildtype RMG1 cells with or without HDAC2 knockdown in 3D culture at day 8. Images were captured using confocal microscopy. Scale bars = 20 μm. (**AA-AB**) Quantification of (Z). 200 cells from each of indicated groups were examined for expression cleaved caspase 3 (AA) or Ki67 (AB). n=3 independent experiments. Error bars represent SEM. *P*-value calculated with two-tailed *t*-test. (**AC**) *ARID1A* wildtype RMG1 cells with or without HDAC2 knockdown were examined for expression of markers of apoptosis cleaved caspase 3 and cleaved PARP p85, HDAC2 and a loading control GAPDH by immunoblot. (**AD-AE**) *ARID1A*-mutated TOV21G cells were transduced with lentivirus encoding the indicated shHDAC2, shEZH2 or a combination. The indicated cells were subjected to colony formation assay. Integrated density of colonies formed by the indicated cells were quantified using the NIH Image J software (AD). n=4 independent experiments. n.s.: not significant. Expression of HDAC2, EZH2, cleaved caspase 3, cleaved PARP p85 and a loading control β-actin was determined by immunoblot (AE).

Supplemental Figure 2

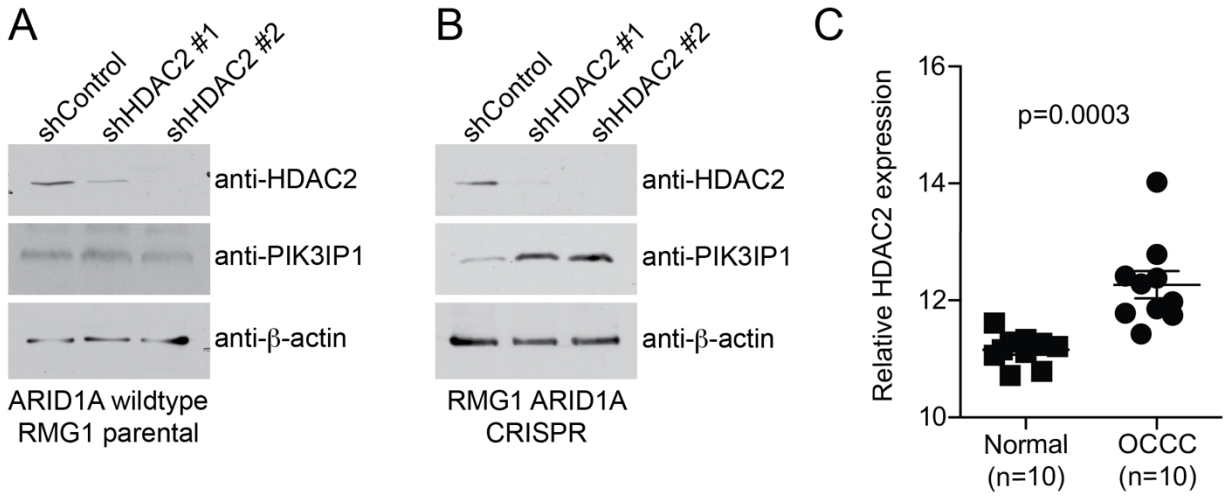

Supplemental Figure 2. HDAC2 regulates PIK3IP1 in an ARID1A-status dependent manner. Related to Figure 2.

(**A-B**) Immunoblot of the indicated proteins in *ARID1A* wildtype RMG1 parental cells or ARID1A CRISPR RMG1 cells with or without HDAC2 knockdown by the indicated shHDAC2s.

(**C**) Relative *HDAC2* mRNA expression in normal human ovarian surface epithelial cells (n = 10) and laser capture and microdissected OCCC tumors (n = 10) based on a published dataset (Stany et al., 2011).

Supplemental Figure 3

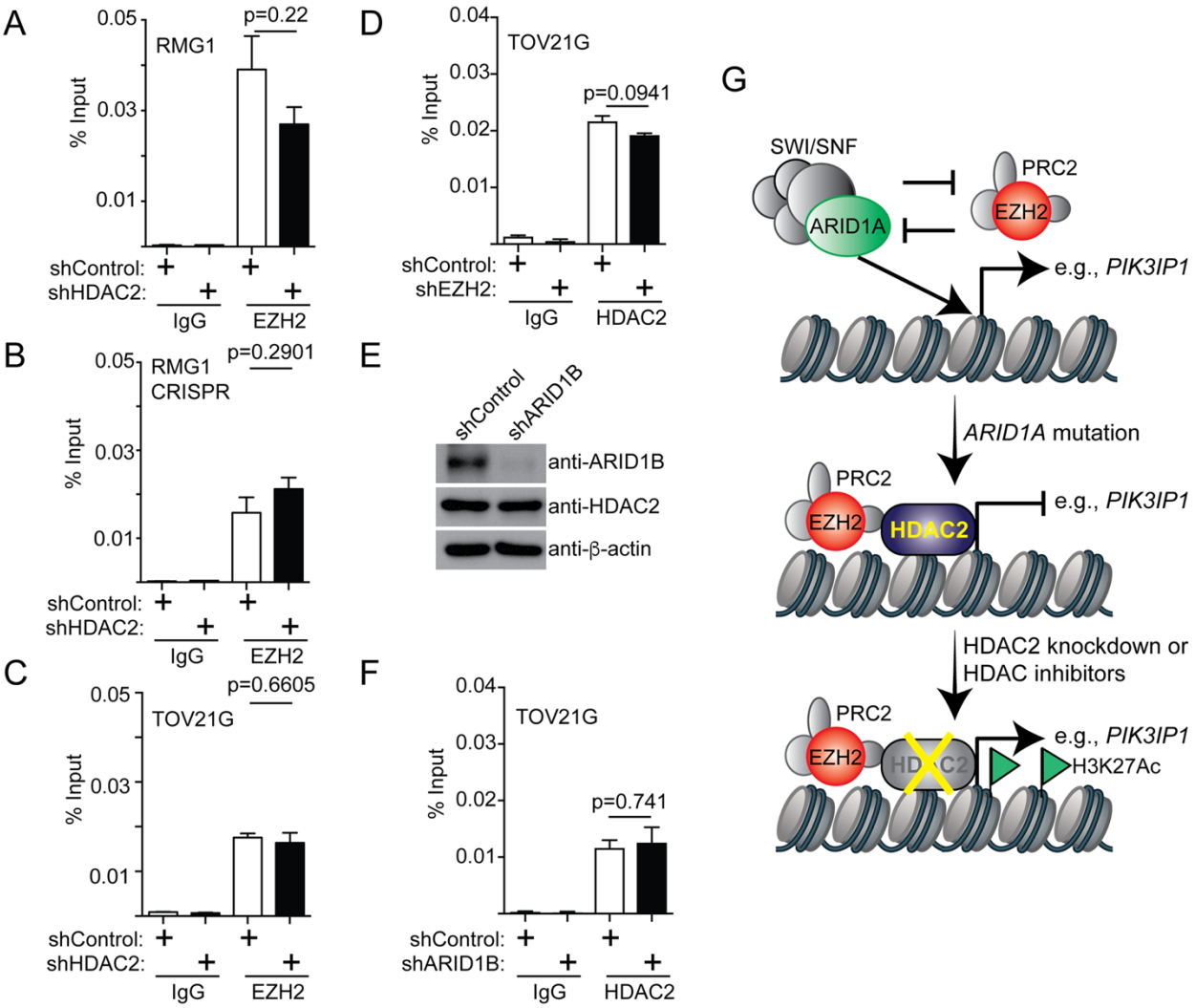

Supplemental Figure 3. HDAC2 does not affect EZH2's association with the *PIK3IP1* gene promoter. Related to Figure 3.

(**A-C**) *ARID1A* wildtype RMG1 cells (A), ARID1A CRISPR RMG1 cells (B) and *ARID1A*-mutated TOV21G cells (C) with or without HDAC2 knockdown were subjected to ChIP analysis for the *PIK3IP* gene promoter using an anti-EZH2 antibody or an isotype-matched IgG control. n=3 independent experiment. Error bars represent SEM. *P*-value calculated with two-tailed *t*-test. (**D**) *ARID1A*-mutated TOV21G cells with or without EZH2 knockdown for 48 hours were subjected to ChIP analysis for the *PIK3IP* gene promoter using an anti-HDAC2 antibody or an isotype-matched IgG control. n=3 independent experiment. Error bars represent SEM. *P*-value calculated with two-tailed *t*-test. Please see Figure S1AD for EZH2 knockdown efficiency. (**E-F**) *ARID1A*-mutated TOV21G with or without ARID1B knockdown for 48 hours were examined for expression of ARID1B, HDAC2 and a loading control β-actin by immunoblot (E), or subjected the cells to ChIP analysis for the *PIK3IP* gene promoter using an anti-HDAC2 antibody or an isotype-matched IgG control (F). n=3 independent experiment. Error bars represent SEM. *P*-value calculated with two-tailed *t*-test. (**G**) A proposed model for the mechanism by which HDAC2 regulates PIK3IP expression in an ARID1A status dependent manner. In *ARID1A* wildtype cells, both ARID1A containing SWI/SNF complex and EZH2 containing PRC2 complex are present in the *PIK3IP1* gene promoter. However, ARID1A dominates over EZH2 in driving the expression of *PIK3IP1* gene in ARID1A wildtype cells. When ARID1A is mutated, HDAC2 is recruited to the *PIK3IP1* gene promoter and functions as a co-repressor of EZH2 to silence the expression of *PIK3IP1*. Accordingly, inhibition of HDAC2 activity by genetic knockdown or HDAC inhibitors reactivates *PIK3IP1* expression, which correlates an increase in H3K27Ac epigenetic mark in the *PIK3IP1* gene promoter.

Supplemental Figure 4

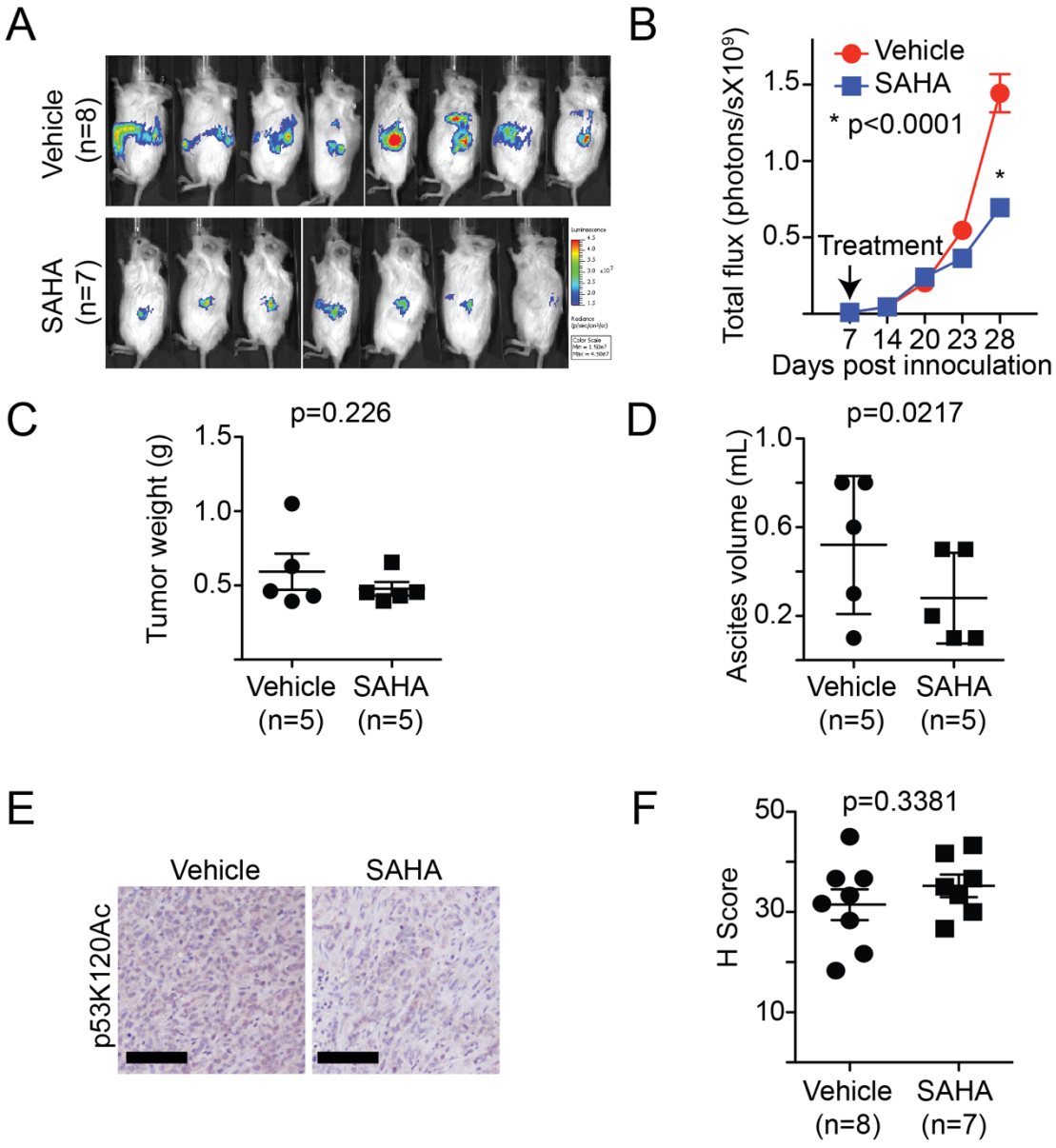

Supplemental Figure 4. SAHA reduced the burden of *ARID1A*-mutated ovarian tumors. Related to Figure 4. (**A-B**) Luciferase expressing *ARID1A*-mutated TOV21G cells were orthotopically injected into the ovarian bursa sac of the NSG female mice. Tumors were allowed to establish for 1 week, and the mice were randomized into two groups based on total luciferase flux. Mice were treated with vehicle control or SAHA (50 mg/kg) daily by i.p. injection for additional three weeks. Mice were imaged weekly. Shown were images taken at day 28 (A). Total flux (photons/sec) was graphed at the indicated time points (B). n=8 mice in vehicle control and n=7 mice in SAHA treated. Error bars represent SEM. *P*-value calculated with two-tailed *t*-test. (**C-D**) Mice with established *ARID1A* wildtype RMG1 tumors were randomized (n=5 mice/group) and treated with vehicle control or SAHA (50 mg/kg) daily by i.p. injection for three weeks. Tumor weigh was quantified and used as a surrogate for tumor burden (C). The volume of ascites produced was quantified (D). Error bars represent SD. *P*-value calculated with two-tailed *t*-test. (**E-F**) Same as (A-B). Consecutive sections of the dissected xenograft tumors were subjected to immunohistochemical (IHC) staining using an anti-lysine 120 acetylated p53 (p53K120Ac) antibody (E). Scale bar = 50 μm. Expression of p53K120Ac was quantified based on H-score for the indicated groups. H-score was based on three different fields from each tumor from each of the indicated groups (F). The number of mice in each of the groups is indicated on the graph. Error bars represent SEM. *P*-value calculated with two-tailed *t*-test.

Supplemental Table Legends

	Names	IC_{50} of SAHA (μM)
ARID1A wildtype	RMG1	0.57
	ES2	1.84
	KK	1.15
	OVCA429	1.97
	XVOA4841	1.42
ARID1A-mutated	TOV21G	0.01
	OVTOKO	0.1
	OVISE	0.03
	SKOV3	0.38
	VOA295	0.04

Supplemental Table 1. SAHA IC_{50} of the listed cell lines and primary cultures. Related to Figure 4.

Supplemental Experimental Procedures

Cell lines and three-dimensional (3D) culture conditions.

The protocol for using primary cultures of human ovarian clear cells was approved by the University of British Columbia Institutional Review Board. The primary tumor cells were cultured in RPMI 1640 supplemented with 10% fetal bovine serum (FBS) and 1% penicillin/streptomycin as previously described (Bitler et al., 2017). Ovarian clear cell carcinoma cell lines (OVISE, TOV21G, RMG1, and OVTOKO cell lines) were all obtained from the Japanese Collection of Research Bioresources. SKOV3 cell line was obtained from the American Type Culture Collection. OVCA429 and KK cell lines were obtained from Dr. Ie-Ming Shih. OVISE, TOV21G, SKOV3, OVCA429, and OVTOKO cells were cultured in RPMI 1640 supplemented with 10% FBS and 1% penicillin/streptomycin. RMG1 cells were cultured in 1:1 Dulbecco's modified Eagle's medium (DMEM): F12 supplemented with 10% FBS and 1% penicillin/streptomycin. KK cell lines were cultured in DMEM supplemented with 10% FBS and 1% penicillin/streptomycin. Cell lines were re-authenticated by The Wistar Institute's Genomics Facility at the end of experiments within the last three months using short tandem repeat profiling using AmpFLSTR Identifier PCR Amplification kit (Life Technologies). Mycoplasma testing was performed by LookOut Mycoplasma PCR detection (Sigma). 3D culture was adapted from previously published methods using growth factor reduced-Matrigel (GFR-Matrigel; BD Biosciences) (Bitler et al., 2015). Briefly, a single cell suspension was plated in 8-well chambers covered with Matrigel. Matrigel media with either vehicle control (DMSO) or drug was changed every 4 days, and cells were grown for 12 days. Each of the experiments was performed in duplicate in three independent experimental repeats.

Reagents and antibodies.

SAHA was obtained from ApexBio Technology LLC. The following antibodies were from the indicated suppliers: anti-HDAC1 (Cell Signaling, Cat. No. 5356, 1:1,000), anti-HDAC2 (Abcam, Cat. No. ab12169, 1:1,000), anti-HDAC2 (Cell Signaling, Cat. No. 2545, 1:1,000), anti-EZH2 (BD Bioscience, Cat. No. 612666, 1:1,000), anti-EZH2 (Cell Signaling, Cat. No. 5246, 1: 1,000), anti-ARID1A (Santa Cruz, Cat. No. sc-32761, 1:500), anti-PIK3IP1 (Santa Cruz, Cat. No. sc-86785, 1:500), anti-H3K27Ace (Millipore, Cat. No. 07-360, 1:1,000), anti-Ki67 (Cell Signaling, Cat. No. 9449, 1:1,000), anti-cleaved caspase 3 (Cell Signaling, Cat. No. 9661, 1: 1,000), anti-cleaved PARP p85 (Promega, Cat. No. G7341, 1: 1,000), anti-pAKT (T308, Cell Signaling, Cat. No. 13038, 1:1,000), anti-AKT (Cell Signaling, Cat. No. 9272, 1:1,000), anti-RNA polymerase Ⅱ (Santa Cruz, Cat. No. sc-899X, 1:500), anti-β-actin (Sigma, Cat. No. A5441, 1:10,000), anti-GAPDH (Millipore, Cat. No. MAB374, 1:10,000). Note that the antibodies against cleaved caspase 3 or cleaved PARP p85 do not recognize the non-cleaved forms of caspase 3 or PARP.

Immunoblotting and Immunoprecipitation

Protein was isolated as previously described (Bitler et al., 2015). Briefly, protein was extracted with RIPA buffer (150mM NaCl, 1% NP40, 0.5% sodium deoxycholate, 0.1% SDS, 50mM Tris pH 8.0, and 1mM PMSF). Protein was separated on a SDS-PAGE and transferred to PVDF membrane. For immunoprecipitation, cells were washed with ice-cold PBS and lysed in the lysis buffer (50 mM Tris-HCl (PH 8.0), 150 mM NaCl, 1 mM EDTA, 0.5% NP40) supplemented with Protease Inhibitor Cocktail (Sigma). The cell lysates were centrifuged at 12000 rpm for 5 min. The supernatant was incubated with indicated antibodies for 3h, followed by incubation with Protein G magnetic Dynabeads for 1 h (Invitrogen). The immunoprecipitated proteins were subsequently analyzed with Immunoblotting. An isotype-matched immunoglobulin G (IgG) was used as a negative control.

Generation of ARID1A CRISPR RMG1 cells.

RMG1 cells were transfected with CRISPR-ARID1A (pSpCas9 (BB)-2A-Puro (PX459)). The ARID1A gRNA 5'- CGGGTTGCCCAGGCTGCTGGCGG-3'. The plasmid was a generous gift from Dr. Cigall Kadoch (DFCI). Fugene6 transfection reagent (Promega) was used as per manufacturer's specifications. Clonal populations for the loss of ARID1A expression were screened through immunoblot as previously described (Bitler et al., 2015).

Lentivirus infection and HDAC2 ectopic expression.

Lentivirus was packaged using the Virapower Kit from Life Technologies (Carlsbad, CA) following the manufacture's instructions. pLenti-CMV-Puro-Luciferase was obtained from Addgene. pLKO.1-shHDAC2 (Cat. No: TRCN0000004819 and TRCN0000004823), pLKO.1-shPIK3IP1 (Cat. No. TRCN0000138560) were from Open Biosystems and obtained from the Molecular Screening Facility at The Wistar Institute. HDAC2 wildtype and a catalytically inactive H142A HDAC2 mutant were constructed by PCR-based mutagenesis using the following

primers. *HDAC2* (forward, 5'-CTCGGATCCATGGCGTACAGTCAAGGAGGCGGCAAAAAAAAAGT-3'; reverse, 5'-GTCCTCGAGTCAGGGGTTGCTGAGCTGTTCTGATTTGG -3')
H142A (forward, 5'-GCTGGAGGATTACATGCTGCTAAGAAATC-3'; reverse, 5'-GATTTCTTAGCAGCATGTAATCCTCCAGC-3') and subcloned into lentivirus plasmid pLVX-Puro (Promega) by BamH1 and Xho1 sites using standard molecular cloning protocols. Cells infected with viruses encoding the puromycin resistance gene were selected 1 μg/ml puromycin.

Reverse-transcriptase quantitative PCR (RT-qPCR).

RNA was extracted from cells with RNeasy Mini Kit followed by on-column DNAse digest (Qiagen). The expression of mRNA levels for *PIK3IP1* (forward, 5' –GCTAGGAGGAACTACCACTTTG -3'; reverse, 5' –GATGGACAAGGAGCACTGTTA -3'), and *HDAC2* (forward, 5'-CATGACCCATAACTTGCTGTTAAA-3'; reverse, 5'-ATCTGGTCTTATTGACCGTAGAAA-3') was determined using SYBR green 1-step iScript (Bio-Rad) with Life Technologies QuantStudio 3. β-2-microglobulin was used as an internal control.

Colony formation assay.

Cell lines were infected with lentivirus pLKO. 1-shRNAs or pLKO. 1-control with puromycin selection marker. Infected cells were selected with 1 μg/mL of puromycin for 72 hours and the selected cells were seeded in 12-well or 24-well plates. Cell medium was changed every three days with appropriate drug doses for 12 days. Colonies were washed twice with PBS and fixed with 10% methanol and 10% acetic acid in distilled water. Fixed colonies were stained with 0.005% crystal violet. Integrated density was measured using NIH ImageJ software.

Immunofluorescence and immunohistochemical staining.

Immunofluorescence was performed after 48 hours as indicated by fixing samples in 4% paraformaldehyde and permeabilizing with 0.5% Triton-X. Samples were incubated with primary antibodies for 2 h at room temperature and with highly cross-absorbed secondary antibodies (Invitrogen) for 1 h at room temperature and mounted with ProLong antifade reagent (Invitrogen). Immuno-stained cells were then imaged using a Leica Confocal microscope. Immunohistochemical staining was performed as described previously (Bitler et al., 2017) on consecutive sections from xenografted tumors dissected from control or SAHA-treated immunocompromised female mice.

RNA-seq and bioinformatics analysis.

For RNA-seq analysis, RNA was extracted from TOV21G cells expressing two individual shHDAC2s or control by Trizol (Invitrogene) and subsequently cleaned and DNase-treated using RNeasy columns (Qiagen). Libraries for RNA-seq were prepared with ScriptSeq complete Gold kit (Epicentre) and subjected to a 75 bp paired-end sequencing run on NextSeq 500, using Illumina's NextSeq 500 high output sequencing kit following the manufacturer's instructions. RNA-seq data was deposited in GEO database (Accession number: GSE107201).

Data from RNA-seq performed on *ARID1A*-mutated TOV21G cells expressing two individual shHDAC2s or control was aligned against hg19 version of genome and Ensemble GRCh37 transcriptome using bowtie2 (Langmead and Salzberg, 2012). RSEM v1.2.12 software (Li and Dewey, 2011) was used to estimate gene level read counts and FPKM values. Only 12599 known genes (with Entrez ID) that had expression level of at least FPKM=1 were considered and EdgeR (Robinson et al., 2010) was used to estimate significance of differential expression difference between the two experimental groups. Upregulated genes with FDR<10% significance threshold were considered. Previously reported ARID1A/EZH2 target genes (Bitler et al., 2015) were overlapped with the list of significantly upregulated genes and significance of overlap was estimated using Hypergeometric test.

Cited references

Bitler, B.G., Aird, K.M., Garipov, A., Li, H., Amatangelo, M., Kossenkov, A.V., Schultz, D.C., Liu, Q., Shih Ie, M., Conejo-Garcia, J.R.*, et al.* (2015). Synthetic lethality by targeting EZH2 methyltransferase activity in ARID1A-mutated cancers. Nat Med *21*, 231-238.

Bitler, B.G., Wu, S., Park, P.H., Hai, Y., Aird, K.M., Wang, Y., Zhai, Y., Kossenkov, A.V., Vara-Ailor, A., Rauscher Iii, F.J.*, et al.* (2017). ARID1A-mutated ovarian cancers depend on HDAC6 activity. Nat Cell Biol *19*, 962-973.

Langmead, B., and Salzberg, S.L. (2012). Fast gapped-read alignment with Bowtie 2. Nat Methods *9*, 357-359.

Li, B., and Dewey, C.N. (2011). RSEM: accurate transcript quantification from RNA-Seq data with or without a reference genome. BMC Bioinformatics *12*, 323.

Pavlik, C.M., Wong, C.Y., Ononye, S., Lopez, D.D., Engene, N., McPhail, K.L., Gerwick, W.H., and Balunas, M.J. (2013). Santacruzamate A, a potent and selective histone deacetylase inhibitor from the Panamanian marine cyanobacterium cf. Symploca sp. J Nat Prod *76*, 2026-2033.

Robinson, M.D., McCarthy, D.J., and Smyth, G.K. (2010). edgeR: a Bioconductor package for differential expression analysis of digital gene expression data. Bioinformatics *26*, 139-140.

Stany, M.P., Vathipadiekal, V., Ozbun, L., Stone, R.L., Mok, S.C., Xue, H., Kagami, T., Wang, Y., McAlpine, J.N., Bowtell, D.*, et al.* (2011). Identification of novel therapeutic targets in microdissected clear cell ovarian cancers. PLoS One *6*, e21121.